crystals

MDPI

Article

Temperature Effects on the Elastic Constants, Stacking Fault Energy and Twinnability of Ni_3Si and Ni_3Ge: A First-Principles Study

Lili Liu [1,2], Liwan Chen [1], Youchang Jiang [1], Chenglin He [1], Gang Xu [1] and Yufeng Wen [3,4,*]

1 Department of Physics, Chongqing Three Gorges University, Chongqing 404100, China; liulili0612@163.com (L.L.); CLW164@126.COM (L.C.); 18581315185@163.com (Y.J.); hcl1965@163.com (C.H.); xugang1978@tom.com (G.X.)
2 Institute for Structure and Function, Chongqing University, Chongqing 401331, China
3 School of Mathematical Sciences and Physics, Jinggangshan University, Ji'an 343009, China
4 School of Materials Science and Engineering, Shanghai Jiaotong University, Shanghai 200240, China
* Correspondence: jgsuwyf@jgsu.edu.cn

Received: 3 August 2018; Accepted: 9 September 2018; Published: 14 September 2018

Abstract: The volume versus temperature relations for Ni_3Si and Ni_3Ge are obtained by using the first principles calculations combined with the quasiharmonic approach. Based on the equilibrium volumes at temperature T, the temperature dependence of the elastic constants, generalized stacking fault energies and generalized planar fault energies of Ni_3Si and Ni_3Ge are investigated by first principles calculations. The elastic constants, antiphase boundary energies, complex stacking fault energies, superlattice intrinsic stacking fault energies and twinning energy decrease with increasing temperature. The twinnability of Ni_3Si and Ni_3Ge are examined using the twinnability criteria. It is found that their twinnability decrease with increasing temperature. Furthermore, Ni_3Si has better twinnability than Ni_3Ge at different temperatures.

Keywords: Ni_3Si; Ni_3Ge; temperature; twinnability; first-principles

1. Introduction

Ni-based single-crystal (SC) superalloys are widely used for turbine blades and vanes in the most advanced gas turbine engines due to their high melting temperature, adequate high temperature strength, elevated thermal stability, excellent oxidation and corrosion resistance [1,2]. The $L1_2$-type ordered phases Ni_3Si and Ni_3Ge exhibit unique mechanical properties which makes them attractive for structural applications at elevated temperatures.

A number of reports, particularly on mechanical properties, have been carried on Ni_3Si and Ni_3Ge. For example, Ochial et al. [3] evaluated the direction of solubility lobe, the extent of homogeneity of $L1_2$ phase and the site preference of ternary additions in Ni_3Ga, Ni_3Si, Ni_3Ge and Ni_3Al through the experiment. Yasuda et al. [4] determined the three elastic stiffness constants of Ni_3X (X = Mn, Fe, Al, Ga, Ge and Si) by the rectangular parallelepiped resonance method. Iotova et al. [5] studied the electronic and mechanical properties of the Ni_3X (X = Mn, Al, Ga, Si, Ge) using first-principles total-energy electronic structure calculations based on the full-potential linear-muffin-tin-orbital method. Chen et al. [6] investigated the structural properties, elastic properties, thermal stability, thermodynamics and electronic structures of Ni_3X (X: Al, Mo, Ti, Pt, Si, Nb, V and Zr) from first-principles calculation. Hou et al. [7] investigated the structural, elastic, thermodynamic and electronic properties of $L1_2$-ordered intermetallic compounds Ni_3X (X = Al, Ga and Ge) under pressure using first-principles methods based on density functional theory. Tanaka et al. [8] measured the elastic-stiffness constants of Ni_3Ga and Ni_3Ge over the temperature range of 77–1200 K using the

rectangular parallelepiped resonance (RPR) method. Prikhodko et al. [9] measured the single-crystal elastic constants of Ni-Ge and Ni-Ga solid solution alloys up to 1100 K. However, the effect of temperature on the dislocation of Ni_3Si and Ni_3Ge have not been reported yet.

It is widely accepted that dislocations play an important role in determining the mechanical properties of the materials [10,11]. Deformation twinning is another deformation mechanism in Ni_3Si and Ni_3Ge. Dislocation-mediated slip and deformation twinning are two major and competing modes of plastic deformation in fcc metals and alloys [12,13]. The generalized stacking fault energy (GSFE) curves play a critical role in revealing the competition between dislocation and deformation twinning. There have been many theoretical studies focused on the qualitative dependence of deformation twinning tendency on the GSFEs in fcc metals and alloys [14–24]. Fu et al. [25] determined the (100) and (111) antiphase boundary (APB) energies and the superlattice intrinsic stacking fault (SISF) energies of Ni_3Si using the first-principle total-energy methods. Mryasov et al. [26] employed the local-density approximation (LDA) and the full-potential linear muffin-tin orbital (FLMTO) method to determine the GSFEs of Ni_3Ge on the $\{111\}$ plane at 0 K. However, the entire GSFE curves and the twinnability of Ni_3Si and Ni_3Ge at different temperatures have not yet been reported. In this paper, the first principles methods and quasiharmonic approximation are used to systematically examine the GSFEs and twinnabilities of Ni_3Si and Ni_3Ge at different temperatures.

2. Method of Calculation

In terms of first-principles quasiharmonic approach, the Helmholtz free energy F for a crystal can be written in the form of

$$F(V,T) = E_0(V) + F_{\mathrm{el}}(V,T) + F_{\mathrm{vib}}(V,T) \tag{1}$$

where $E_0(V)$ is the static energy at 0 K and F_{el} is the thermal electronic contribution to free energy from finite temperature. Both the $E_0(V)$ and F_{el} can be obtained from first principles calculations. F_{vib} is the vibrational free energy of the lattice atoms given by

$$F_{\mathrm{vib}}(V,T) = \sum_{\kappa}\left\{\frac{1}{2}\hbar\omega_{\kappa}(V) + k_B T \ln\left[1 - \exp\left(-\frac{\hbar\omega_{\kappa}(V)}{k_B T}\right)\right]\right\} \tag{2}$$

where k_B is the Boltzmann constant, $\hbar$ is the reduced Planck constant, ω_{κ} represents an individual phonon frequency.

The isothermal elastic constants C_{ij}^T, with respect to the finite strain variables, are defined as [27]

$$C_{ij}^T = \frac{1}{V}\frac{\partial^2 F}{\partial\eta_i\eta_j}\Big|_{T,\eta'} \tag{3}$$

where $V = V(T)$ is the volume at temperature T and η' represents that all other strains are held fixed. For a cubic system, there are three independent elastic constants C_{11}^T, C_{12}^T and C_{44}^T. The bulk modulus B_T determined from the Vinet equation of state [28] is approximated by the combinations of the elastic moduli

$$B_T^T = (C_{11}^T + 2C_{12}^T)/3 \tag{4}$$

A volume-conserving orthorhombic strain is applied to determine the difference between the C_{11}^T and C_{12}^T

$$\eta(\xi) = \begin{pmatrix} \xi & 0 & 0 \\ 0 & \xi & 0 \\ 0 & 0 & (1+\xi)^{-2} - 1 \end{pmatrix} \tag{5}$$

which leads to the Helmholtz free energy change

$$F(V,\xi) = F(V,0) + 3(C_{11}^T - C_{12}^T)V\xi^2 + O(\xi^3) \tag{6}$$

A volume-conserving tetragonal strain is applied to determine C_{44}^T

$$\eta(\xi) = \begin{pmatrix} 0 & \xi & 0 \\ \xi & 0 & 0 \\ 0 & 0 & \xi^2/(1-\xi^2) \end{pmatrix} \tag{7}$$

and the corresponding Helmholtz free energy change is

$$F(V,\xi) = F(V,0) + 2C_{44}^T V\xi^2 + O(\xi^4) \tag{8}$$

In present work, a first-principles quasistatic approach proposed by Wang et al. [29,30] is employed to determine the temperature dependent elastic constants $C_{ij}(T)$. In this approach, the change of elastic constants at higher temperature is mainly caused by volume change. The temperature dependence of the elastic constants $C_{ij}(T)$ can be estimated by the application of the following three-step procedure. In the first step, the equilibrium volume $V(T)$ at given T is obtained by employing the first-principles quasiharmonic approach. In the second step, the static elastic constants at 0 K as a function of volume are obtained by using the energy-strain relations based on Equations (4)–(8). In the third step, the calculated elastic constants from the second step at the volume are estimated as those at finite temperature. The elastic constants at higher temperature are usually measured by the resonance method. That is, the crystal system is adiabatic because elastic waves travel faster than heat diffuses and the deformation can be viewed as a isoentropic process [31]. Thus, the isothermal elastic constants C_{ij}^T need to be transformed to the adiabatic elastic constants C_{ij}^S by the following relation

$$C_{11}^S = C_{11}^T + \frac{TV}{C_V}\alpha^2 B_T^2 \tag{9}$$

$$C_{12}^S = C_{12}^T + \frac{TV}{C_V}\alpha^2 B_T^2 \tag{10}$$

$$C_{44}^S = C_{44}^T \tag{11}$$

where C_V is the specific heat at constant volume, and α is the volume thermal expansion coefficient obtained by $\alpha(T) = \frac{1}{V}(\frac{dV(T)}{dT})$.

In this work, all calculations were performed using the VASP code [32–34], which is based on the implementation of density functional theory with the exchange-correlation functional depicted by the generalized gradient approximation (GGA) in the Perdew–Burke–Ernzerhof (PBE) [35]. The ion electron interaction is described by the plane-wave basis projector augmented wave (PAW) method [36,37]. For calculation of the GSFEs of Ni_3Si and Ni_3Ge at different temperatures, a periodic supercell consisting of ten atomic planes is employed. Between the periodically repeated supercell a vacuum space with six atomic layers is added to avoid interactions between faults in two neighboring slabs. A plane wave basis set with energy cutoff of 550 eV is used for all calculations. Brillouin zone (BZ) integrations are performed using the Monkhorst–Pack special k-point scheme [38]. The samplings of k meshes are $15 \times 15 \times 15$ for lattice and elastic constants calculations and $15 \times 15 \times 1$ for generalized stacking fault energy calculations. The self-consistent convergence of the total energy is set to 10^{-6} eV/atom and the maximum force on the atom is 10^{-4} eV/Å.

Phonon calculations are carried out by the supercell approach within the framework of force-constant method. The chosen supercell size strongly influences on the thermal properties.

After a lot of testing, the adequate supercell size consisting of 3 × 3 × 3 unit cells with 108 atoms is good enough for calculating the phonon dispersions. The forces acting on atoms for each perturbed supercell are calculated by VASP with 5 × 5 × 5 for Ni_3Si and Ni_3Ge. Phonon dispersion curves for Ni_3Si and Ni_3Ge along high-symmetry directions in the Brillouin zone are plotted in Figure 1. The Helmholtz free energy curves as a function of unit cell volume with a step of 100 K from 0 to 900 K at 14 volume points are given in Figure 2. At each temperature point, the equilibrium volume V depicted by the red triangle is obtained by minimizing the Helmholtz free energy with respect to V from fitting the integral form of the Vinet equation of state (EOS) [28]. The specific details of calculating the phonon and thermodynamic properties can be found in Refs. [39] and [40].

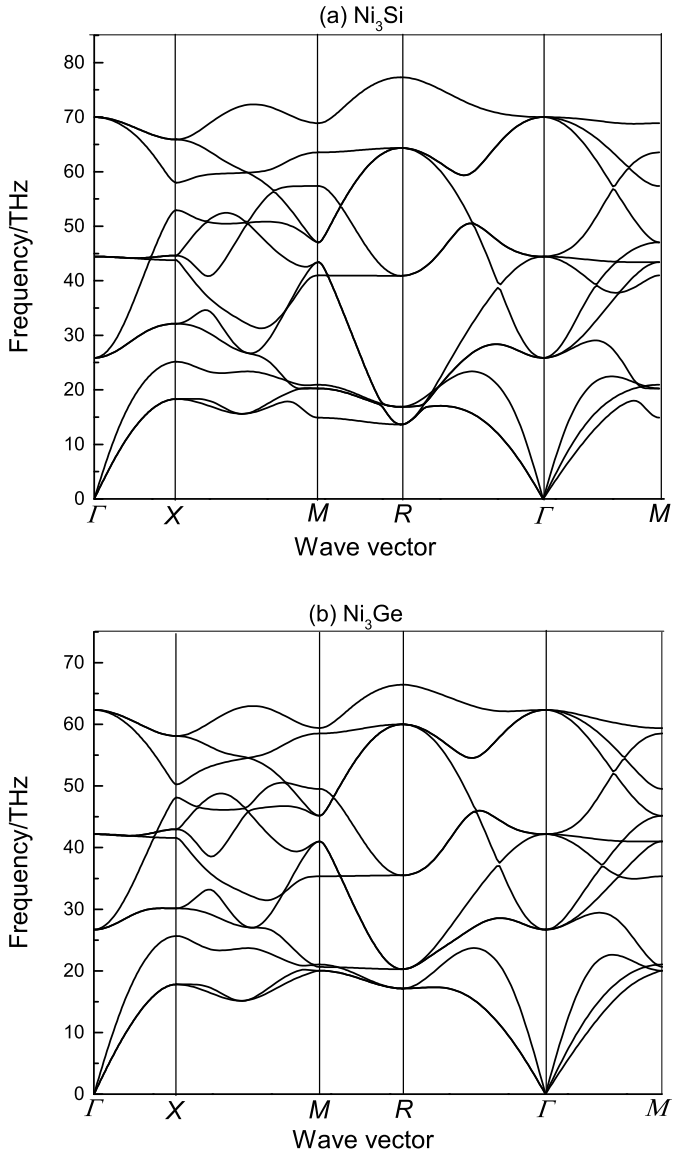

Figure 1. Phonon spectra of (**a**) Ni_3Si and (**b**) Ni_3Ge along high-symmetry directions in the Brillouin zone.

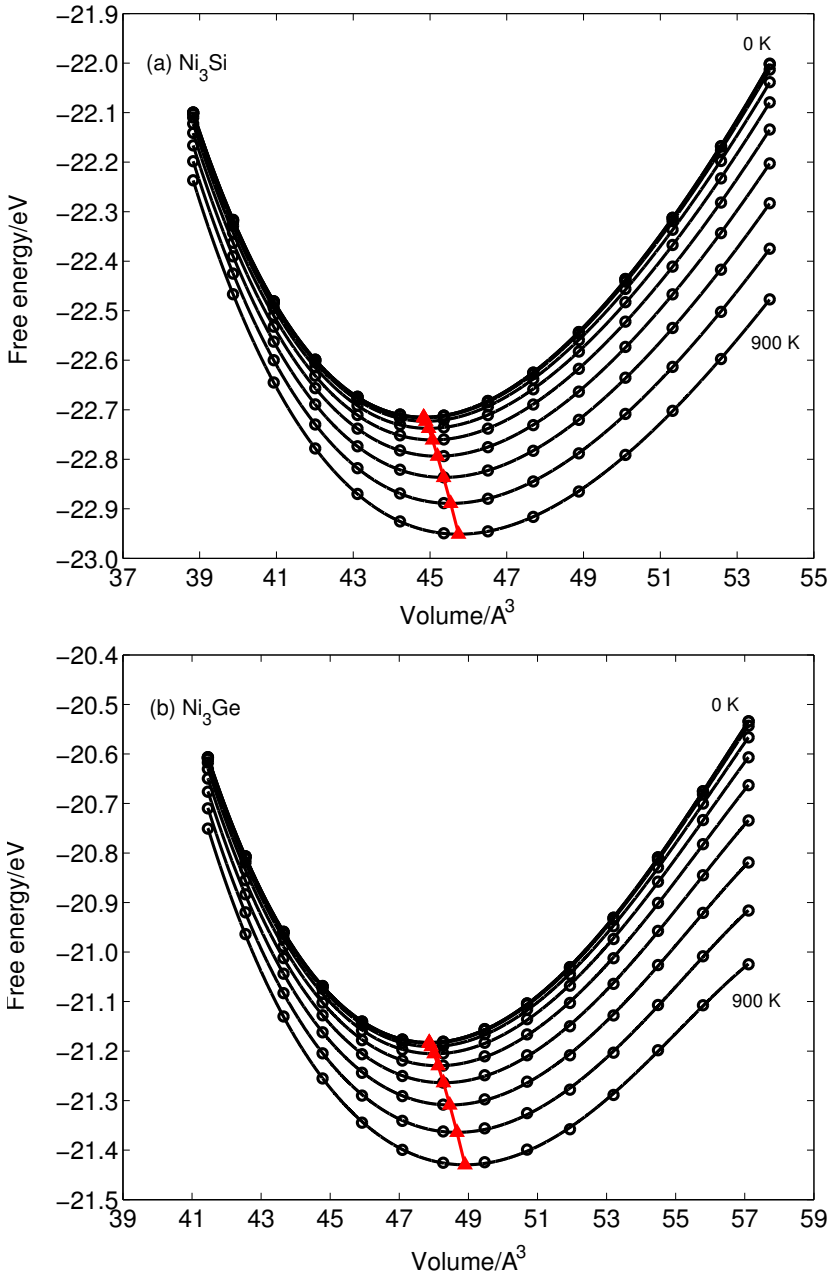

Figure 2. The values of Helmholtz free energy as a function of unit cell volume of (**a**) Ni_3Si and (**b**) Ni_3Ge at every 100 K between 0 and 900 K. The red triangles indicate the corresponding equilibrium volumes at temperatures.

3. Results and Discussion

The calculated lattice constants and isentropic elastic constants C_{ij}^S at $T = 0$ K are listed in Table 1, along with the available experimental and theoretical values. It can be seen that the calculated values in this work are consistent with the theoretical calculations [6,7] at 0 K and experimental values [4] at room temperature. The temperature dependent elastic constants are important for understanding and predicting the mechanical strength, stability and phase transitions of a material [41]. Figure 3 shows the predicted isoentropic elastic constants of Ni_3Si and Ni_3Ge as a function of temperature in the temperature range of 0–900 K. It can be seen that all the values are almost invariant at low temperatures and decrease with increasing temperature at high temperatures. C_{11}^S represents the elasticity in length, whereas C_{12}^S and C_{44}^S are related to the elasticity in shape. Whatever Ni_3Si or Ni_3Ge, it can be seen

that C_{11}^S decreases to the largest extant within the temperature range of the study. C_{11}^S, C_{12}^S and C_{44}^S for Ni_3Si decrease by 18.3, 9.7 and 10.2 GPa, and those for Ni_3Ge decrease by 18.9, 11.1 and 8.9 GPa, respectively. The elastic constants of Ni_3Si and Ni_3Ge compounds at different temperatures satisfy the mechanical stability criteria in a cubic crystal [42]: $C_{11} - C_{12} > 0$, $C_{11} > 0$ and $C_{44} > 0$, which indicates that they are mechanically stable in the temperature range of 0–900 K.

Table 1. Calculated lattice parameter a and elastic constants C_{11}, C_{12}, C_{44} of Ni_3Si and Ni_3Ge at 0 K compared with the previous theoretical and experimental data.

Materials	Ref.	a	C_{11}	C_{12}	C_{44}
Ni_3Si	This work	3.553	268.5	140.4	107.5
	[6]	3.517	317	162	129
Ni_3Ge	This work	3.629	235.3	130.6	85.2
	[7]	3.584	268.9	148.4	103.4
	[4]		263.0	143.0	103.0

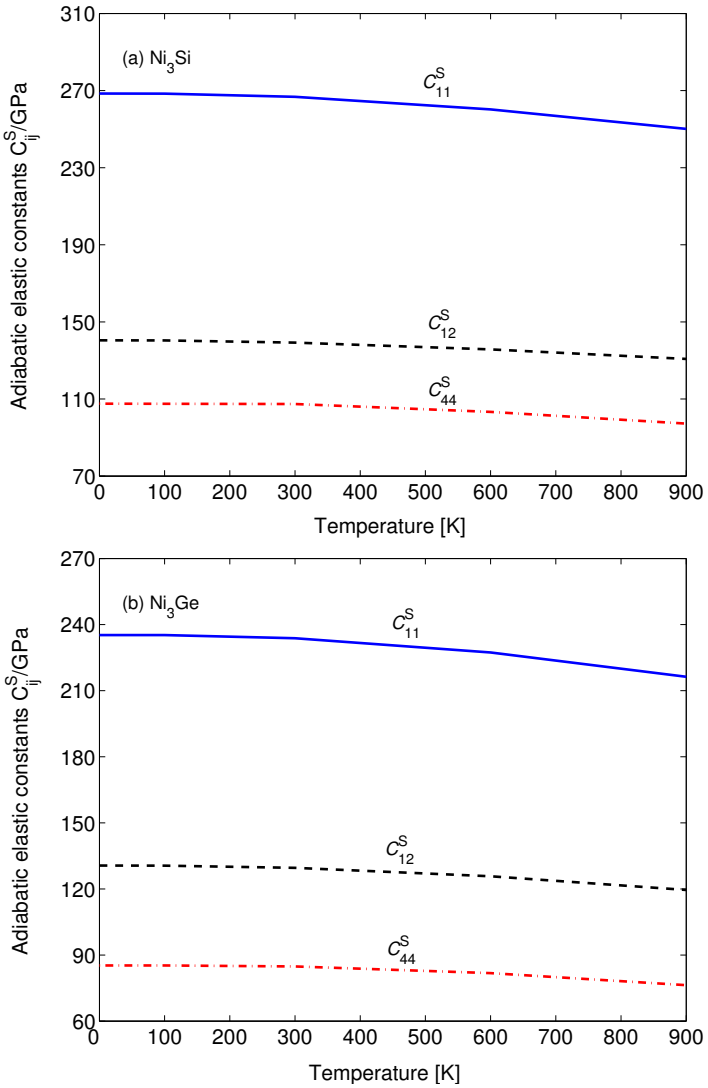

Figure 3. The predicted isentropic elastic constants as a function of temperature for (**a**) Ni_3Si and (**b**) Ni_3Ge, respectively. The C_{11}^S, C_{12}^S and C_{44}^S are represented by the solid, dashed and dashed-dotted curves, respectively.

The plastic behavior of Ni_3Si and Ni_3Ge is mainly determined by the dislocation motion and deformation twinning. The (001) and (111) planes are the two primary slip planes in $L1_2$ structure [43]. It is widely accepted that there are three different types of dislocation dissociations in Ni_3Si and Ni_3Ge. In the (111) or (001) plane, a $[\bar{1}0\bar{1}]$ superdislocation will collinearly dissociated into two $1/2[\bar{1}0\bar{1}]$ superpartials bound by an APB as following reaction:

$$[\bar{1}0\bar{1}] \rightarrow \frac{1}{2}[\bar{1}0\bar{1}] + \mathrm{APB} + \frac{1}{2}[\bar{1}0\bar{1}] \tag{12}$$

where $[\bar{1}0\bar{1}]$ is the Burgers vector of perfect superdislocations in (111) and (001) planes. Furthermore, the $[\bar{1}0\bar{1}]\{111\}$ superpartial may further dissociate into two $1/6\langle 112\rangle$ Schockley partials separated by two complex stacking faults (CSF), which is called as a metastable dissociated dissociation, namely

$$[\bar{1}0\bar{1}] \rightarrow \frac{1}{6}[\bar{1}\bar{1}2] + \mathrm{CSF} + \frac{1}{6}[\bar{2}11] + \mathrm{APB} + \frac{1}{6}[\bar{1}\bar{1}2] + \mathrm{CSF} + \frac{1}{6}[\bar{2}11] \tag{13}$$

The $[\bar{1}0\bar{1}]\{111\}$ perfect superdislocations may be also divided into $1/3\langle 112\rangle\{111\}$ superpartials with a superlattice intrinsic stacking fault (SISF), namely,

$$[\bar{1}0\bar{1}] \rightarrow \frac{1}{3}[\bar{2}11] + \mathrm{SISF} + \frac{1}{3}[\bar{1}\bar{1}2] \tag{14}$$

In this work, on the basis of the temperature dependent lattice constants $a(T)$, all the calculated stacking fault energies of Ni_3Si and Ni_3Ge as a function of temperature are given in Figures 4 and 5, respectively. The discrete points denote the values of first principles calculations and the solid curves represent the results obtained from polynomial fitting. All the various typical energies (γ_{us}, γ_{CSF}, γ_{SISF}, γ_{APB}) at different temperatures for Ni_3Si and Ni_3Ge are listed in Table 2, respectively. The γ_{us} is the unstable stacking fault energy, which is an important solid state parameter that demonstrates the resistance to dislocation nucleation in materials [44,45]. The present results ($\gamma_{APB}^{\{111\}}$ = 599 mJ/m^2, $\gamma_{SISF}^{\{111\}}$ = 308 mJ/m^2 and $\gamma_{CSF}^{\{111\}}$ = 610 mJ/m^2 for Ni_3Si, $\gamma_{APB}^{\{111\}}$ = 622 mJ/m^2, $\gamma_{SISF}^{\{111\}}$ = 306 mJ/m^2 and $\gamma_{CSF}^{\{111\}}$ = 609 mJ/m^2 for Ni_3Ge) at 0 K agree with the results ($\gamma_{APB}^{\{111\}}$ = 625 mJ/m^2, $\gamma_{SISF}^{\{111\}}$ = 460 mJ/m^2 and $\gamma_{CSF}^{\{111\}}$ = 710 mJ/m^2 for Ni_3Si) obtained by Yoo et al. [46] through the first principles total-energy calculations within the framework of the local-density functional theory and the results ($\gamma_{APB}^{\{111\}}$ = 660 mJ/m^2, $\gamma_{SISF}^{\{111\}}$ = 420 mJ/m^2 and $\gamma_{CSF}^{\{111\}}$ = 620 mJ/m^2 for Ni_3Ge) obtained by Mryasov et al. [26] through the ab-initio calculations. However, there are no experimental and theoretical values of stacking fault energies at finite temperature for comparison. For Ni_3Si and Ni_3Ge, it can be found that all the stacking fault energies decrease with increasing temperature, since thermal expansion may soften the stacking fault configuration at higher temperatures. From Table 2, it is easily found that the γ_{us} along the $\langle 112\rangle\{111\}$ is the lowest, indicating that the emission of a dislocation is most likely at this slip system.

Generally, there are no deformation twinning in Ni_3Si and Ni_3Ge intermetallic compounds. However, the deformation micro-twinning can be observed in the precipitation phases of the Ni_3Si and Ni_3Ge intermetallic compounds at higher temperature. There are two types of deformation twinning in Ni_3Si and Ni_3Ge. One is pseudo-twinning and the other is anti-twinning. The former is generated by the sequential motions of identical $1/6\langle\bar{2}11\rangle$ Shockley's partial dislocations and the latter is formed by sequential shear of $1/3\langle\bar{1}2\bar{1}\rangle$ dislocations on successive (111) planes. The $1/6\langle\bar{2}11\rangle$ Shockley's partial dislocation is easy to form, but the formation of the $1/3\langle\bar{1}2\bar{1}\rangle$ dislocation is very difficult. Besides, the dislocations of the disordered solid solution matrix phase of nickel-based superalloys are also the $1/6\langle\bar{2}11\rangle$ Shockley's partial dislocations. Therefore, the generalized planar fault energy (GPFE) curves along the $1/6\langle\bar{2}11\rangle$ pseudo-twinning direction at different temperatures for Ni_3Si and Ni_3Ge are plotted in Figure 6. The first half of each GPFE curve is created by sliding the upper 6–10 atomic layers relative to the lower 1–5 layers along $\langle\bar{2}11\rangle$ over a distance $a/\sqrt{6}$ and

the stacking fault $\cdots$ABCABCBCABCA$\cdots$ is generated. The second half is then constructed by displacing the upper 7–10 layers in a similar fashion and the two-layer twin $\cdots$ABCABCBABCAB$\cdots$ is generated. For each GPFE curve, the first maximum value is the unstable stacking fault energy γ_{us1} and the second maximum value is the unstable twinning energy γ_{ut}, the first minimum value is the intrinsic stacking fault energy γ_{sf} and the second minimum value is the twin stacking fault energy $2\gamma_{tsf}$. Numerical values extracted from the curves' extrema are listed in Table 2. All these values decrease with increasing temperature.

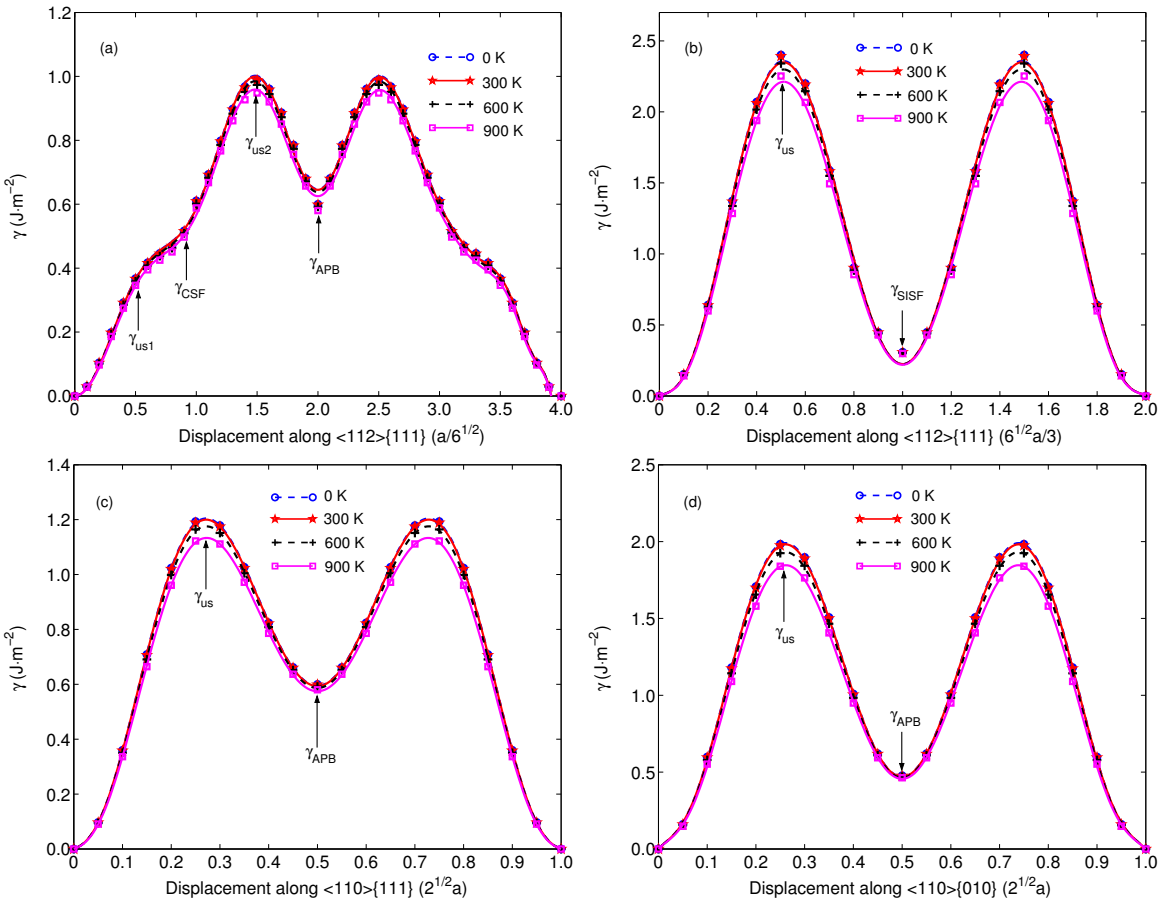

Figure 4. The calculated generalized stacking fault energy curves for Ni_3Si (**a**) sliding along $\langle 112\rangle\{111\}$ $(a/6^{1/2})$, (**b**) sliding along $\langle 112\rangle\{111\}$ $(6^{1/2}a/3)$, (**c**) sliding along $\langle 110\rangle\{111\}$ $(2^{1/2}a)$ and (**d**) sliding along $\langle 110\rangle\{010\}$ $(2^{1/2}a)$. The discrete points represent the results from first-principles calculations and the curves denote the results from polynomial fitting.

Van Swygenhoven et al. [14] proposed that the difference $\delta_{us}^{ut} \equiv \gamma_{ut} - \gamma_{us}$ can estimate the ease with which an fcc material deforms by twinning relative to deforming by dislocation-mediated slip. Tadmor and Bernstein [15] proposed a more thorough treatment of the balance between dislocation mediated slip and deformation twinning, that is

$$\tau_a = \left[1.136 - 0.151\frac{\gamma_{sf}}{\gamma_{us}}\right]\sqrt{\frac{\gamma_{us}}{\gamma_{ut}}} \tag{15}$$

where γ_{sf} and γ_{us} are replaced by γ_{CSF} and γ_{us1} for the pseudo-twinning in Ni_3Si and Ni_3Ge intermetallic compounds, respectively. τ_a is called as the twinnability parameter of a crystal. $\tau_a > 1$ indicates that the main deformation mechanism is the deformation twinning, $\tau_a < 1$ shows that the main deformation mechanism is the dislocation slip and $\tau_a = 1$ demonstrates that the main deformation mechanism is the full dislocation movement. Besides, a larger τ_a indicates a greater

propensity for twinning. All the values of δ_{us}^{ut} and τ_a at different temperatures for Ni_3Si and Ni_3Ge are listed in Table 2. Obviously, both δ_{us}^{ut} and τ_a decrease with increasing temperature. Whatever Ni_3Si or Ni_3Ge, the values of δ_{us}^{ut} are always larger than 0 in the temperature range of 0–900 K. This phenomenon demonstrates that the main deformation mechanism does not change with increasing temperature, but the twinnability of Ni_3Si and Ni_3Ge increase with increasing temperature. From Table 2, it can be seen that the twinnability parameters of Ni_3Si (τ_a = 0.550) and Ni_3Ge (τ_a = 0.500) at 0 K are much smaller than those of the fcc pure metals Al (τ_a = 0.930), Cu (τ_a = 1.001) and Ag (τ_a = 1.042) [15]. However, the twinnability of Ni_3Si and Ni_3Ge are similar to that of Ni_3Al. Besides, the twinnability parameters of Ni_3Si and Ni_3Ge are smaller than 1 in the whole temperature and their twinnability parameters decrease with increasing temperature, which indicates that it is difficult to form the pseudo-twinning through the direct shearing and the twinnability of Ni_3Si and Ni_3Ge decrease with increasing temperature. That is to say, the twinnability of Ni_3Si and Ni_3Ge with temperature predicted by τ_a and δ_{us}^{ut} are different. The twinnability criterion τ_a is dependent on the γ_{ut} and γ_{us} in addition to γ_{sf}, but δ_{us}^{ut} is based on the γ_{ut} and γ_{us}. Therefore, τ_a can more accurately describe the twinnability of a material in comparison with δ_{us}^{ut}. Furthermore, the twinnability of Ni_3Si is greater than that of Ni_3Ge at different temperatures according to the two criteria τ_a and δ_{us}^{ut}. This may be resulted from that the difference between γ_{ut} and γ_{us} of Ni_3Ge is greater than that of Ni_3Si.

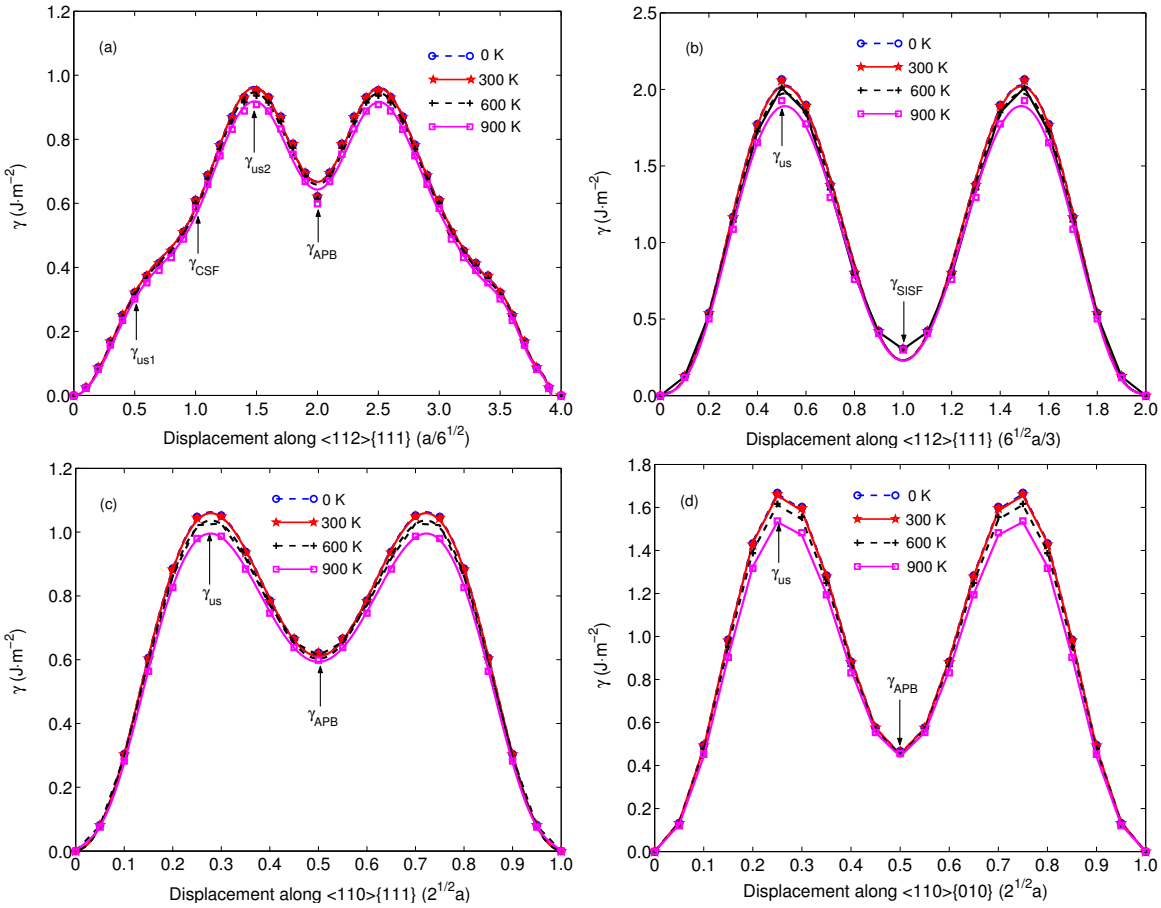

Figure 5. The calculated generalized stacking fault energy curves for Ni_3Ge (**a**) sliding along $\langle 112 \rangle \{111\}$ ($a/6^{1/2}$), (**b**) sliding along $\langle 112 \rangle \{111\}$ ($6^{1/2}a/3$), (**c**) sliding along $\langle 110 \rangle \{111\}$ ($2^{1/2}a$) and (**d**) sliding along $\langle 110 \rangle \{010\}$ ($2^{1/2}a$). The discrete points represent the results from first-principles calculations and the curves denote the results from polynomial fitting.

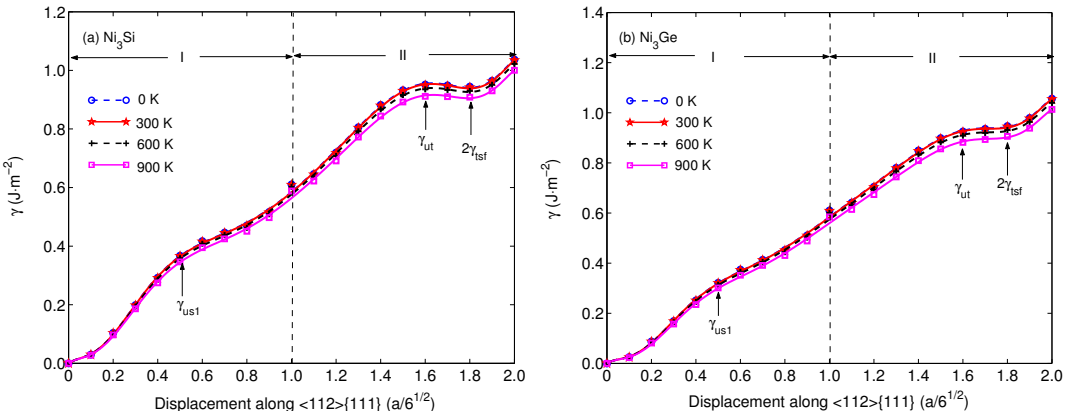

Figure 6. Temperature effects on the generalized planar fault energy curves of (**a**) Ni_3Si and (**b**) Ni_3Ge, respectively. The discrete points denote the values from first-principles calculations and the curves represent the results from polynomial fitting.

Table 2. Calculated various fault energies (J/m^2), relative barrier difference $\delta_{us}^{ut} \equiv \gamma_{ut} - \gamma_{us}$ (J/m^2) and twinnability τ_a at different temperatures of Ni_3Si and Ni_3Ge.

Ni_3Si	T (K)	0	300	600	900
	$\gamma_{us1}^{\langle 112\rangle\{111\}}$	0.367	0.366	0.359	0.346
	$\gamma_{us2}^{\langle 112\rangle\{111\}}$	0.990	0.988	0.973	0.948
	$\gamma_{us}^{\langle 110\rangle\{111\}}$	1.193	1.189	1.164	1.122
	$\gamma_{CSF}^{\langle 112\rangle\{111\}}$	0.610	0.609	0.602	0.588
	$\gamma_{SISF}^{\langle 112\rangle\{111\}}$	0.308	0.307	0.304	0.298
	$\gamma_{ut}^{\langle 112\rangle\{111\}}$	0.951	0.949	0.935	0.911
	$2\gamma_{tsf}^{\langle 112\rangle\{111\}}$	0.944	0.942	0.929	0.908
	$\gamma_{us}^{\langle 110\rangle\{010\}}$	1.984	1.975	1.925	1.840
	$\gamma_{APB}^{\{111\}}$	0.599	0.598	0.592	0.580
	$\gamma_{APB}^{\{010\}}$	0.477	0.476	0.471	0.463
	δ_{us}^{ut}	0.584	0.583	0.576	0.565
	τ	0.550	0.549	0.547	0.541
Ni_3Ge	T (K)	0	300	600	900
	$\gamma_{us1}^{\langle 112\rangle\{111\}}$	0.321	0.320	0.314	0.301
	$\gamma_{us2}^{\langle 112\rangle\{111\}}$	0.953	0.951	0.936	0.908
	$\gamma_{us}^{\langle 110\rangle\{111\}}$	1.047	1.044	1.021	0.980
	$\gamma_{CSF}^{\langle 112\rangle\{111\}}$	0.609	0.608	0.600	0.584
	$\gamma_{SISF}^{\langle 112\rangle\{111\}}$	0.306	0.305	0.303	0.298
	$\gamma_{ut}^{\langle 112\rangle\{111\}}$	0.925	0.923	0.908	0.882
	$2\gamma_{tsf}^{\langle 112\rangle\{111\}}$	0.947	0.944	0.931	0.906
	$\gamma_{us}^{\langle 110\rangle\{010\}}$	1.667	1.661	1.617	1.537
	$\gamma_{APB}^{\{111\}}$	0.622	0.620	0.613	0.598
	$\gamma_{APB}^{\{010\}}$	0.466	0.465	0.462	0.456
	δ_{us}^{ut}	0.604	0.603	0.594	0.581
	τ	0.500	0.499	0.498	0.492

4. Conclusions

In this work, temperature effects on the elastic constants, generalized stacking fault energies and generalized planar fault energies of Ni_3Si and Ni_3Ge are investigated by the first principles calculations combined with a quasiharmonic approach. It is found that the elastic constants, APB energies, CSF energies, SISF energies and twinning energy decrease with increasing temperature. Besides, the twinnability of Ni_3Si and Ni_3Ge with temperature have been investigated through the two criteria τ_a and δ_{us}^{ut}, but the two criteria give different results. τ_a is dependent on the γ_{ut} and γ_{us} in addition to γ_{sf}, but δ_{us}^{ut} is based on γ_{ut} and γ_{us}, that is to say, τ_a can more accurately give the twinnability of a material. Furthermore, the twinnability of Ni_3Si is greater than that of Ni_3Ge at different temperatures.

Author Contributions: L.C. and Y.J. carried out the theoretical calculations; L.L. and G.X. analyzed the data; Y.W. and C.H. wrote the paper.

Funding: The work is supported by the Science and Technology Research Program of Chongqing Municipal Education Commission (Grant No. KJ1710252), the Talent Introduction Project of Chongqing Three Gorges University (Grant No. 16RC06), the Natural Science Foundation of China (51661013, 11464020) and the PhD Start-up Fund of Natural Science Foundation of Jinggangshan University (JZB15007).

Conflicts of Interest: The authors declare no conflict of interest.

References

1. Reed, R.C. *The Superalloys: Fundamentals and Applications*; Cambridge University Press: Cambridge, UK, 2006.
2. Sims, C.T.; Stoloff, N.S.; Hagel, W.C. *Superalloys II*; Wiley: New York, NY, USA, 1987.
3. Ochial, S.; Oya, Y.; Suzuki, T. Alloying behaviour of Ni_3Al, Ni_3Ga, Ni_3Si and Ni_3Ge. *Acta Metall.* **1984**, *32*, 289–298. [CrossRef]
4. Yasuda, H.; Takasugi, T.; Koiwa, M. Elasticity of Ni-based L12-type intermetallic compounds. *Acta Metall. Mater.* **1992**, *40*, 381–387. [CrossRef]
5. Iotova, D.; Kioussis, N.; Lim, S.P. Electronic structure and elastic properties of the Ni_3X (X = Mn, Al, Ga, Si, Ge) intermetallics. *Phys. Rev. B* **1996**, *54*, 14413. [CrossRef]
6. Chen, Q.; Huang, Z.W.; Zhao, Z.D.; Hu, C.K. First-principles study on the structural, elastic, and thermodynamics properties of Ni_3X (X: Al, Mo, Ti, Pt, Si, Nb, V, and Zr) intermetallic compounds. *Appl. Phys. A* **2014**, *116*, 1161–1172. [CrossRef]
7. Hou, H.; Wen, Z.Q.; Zhao, Y.H.; Fu, L.; Wang, N.; Han, P.D. First-principles investigations on structural, elastic, thermodynamic and electronic properties of Ni_3X (X = Al, Ga and Ge) under pressure. *Intermetallics* **2014**, *44*, 110–115. [CrossRef]
8. Tanaka, K.; Yasuda, H.; Koiwa, M. Temperature Dependence of Elastic Constants of Several Intermetallic Compounds. In Proceedings of the 3rd Japan International SAMPE, Chiba, Japan, 7–10 December 1993.
9. Prikhodko, S.V.; Isaak, D.G.; Fisher, E.; Starostina, N.V.; Ma, Y.; Ardell, A.J. The elastic constants of FCC Ni-Ga and Ni-Ge alloys up to 1100 K. *Scr. Mater.* **2006**, *54*, 1327–1330. [CrossRef]
10. Hirth, J.P.; Lothe, J. *Theory of Dislocations*, 2nd ed.; Wiley: New York, NY, USA, 1982.
11. Schoeck, G. The Peierls model: Progress and limitations. *Mater. Sci. Eng. A* **2005**, *400*, 7–17. [CrossRef]
12. Christian, J.W.; Mahajan, S. Deformation twinning. *Prog. Mater. Sci.* **1995**, *39*, 1–157. [CrossRef]
13. Xie, H.X.; Wang, C.Y.; Yu, T.; Du, J.P. Dislocation formation and twinning from the crack tip in Ni_3Al: Molecular dynamics simulations. *Chin. Phys. B* **2009**, *18*, 251–258.
14. van Swygenhoven, H.; Derlet, P.M.; Froseth, A.G. Stacking fault energies and slip in nanocrystalline metals. *Nat. Mater.* **2004**, *3*, 399. [CrossRef] [PubMed]
15. Tadmor, E.B.; Bernstein, N. A first-principles measure for the twinnability of FCC metals. *J. Mech. Phys. Solids* **2004**, *52*, 2507–2519. [CrossRef]
16. Siegel, D.J. Generalized stacking fault energies, ductilities, and twinnabilities of Ni and selected Ni alloys. *Appl. Phys. Lett.* **2005**, *87*, 121901. [CrossRef]
17. Kibey, S.; Liu, J.B.; Johnson, D.D.; Sehitoglu, H. Generalized planar fault energies and twinning in Cu-Al alloys. *Appl. Phys. Lett.* **2006**, *89*, 191911. [CrossRef]
18. Kibey, S.; Liu, J.B.; Johnson, D.D.; Schitoglu, H. Energy pathways and directionality in deformation twinning. *Appl. Phys. Lett.* **2007**, *91*, 181916. [CrossRef]
19. Muzyk, M.; Pakiela, Z.; Kurzydlowski, K.J. Ab initio calculations of the generalized stacking fault energy in aluminium alloys. *Scr. Mater.* **2011**, *64*, 916–918. [CrossRef]
20. Li, B.Q.; Sui, M.L.; Mao, S.X. Twinnability predication for fcc metals. *J. Mater. Sci. Technol.* **2011**, *27*, 97–100. [CrossRef]
21. Wen, Y.F.; Sun, J. Generalized planar fault energies and mechanical twinning in gamma TiAl alloys. *Scr. Mater.* **2013**, *68*, 759–762. [CrossRef]
22. Shang, S.L.; Wang, W.Y.; Zhou, B.C.; Wang, Y.; Darling, K.A.; Kecskes, L.J.; Mathaudhu, S.N.; Liu, Z.K. Generalized stacking fault energy, ideal strength and twinnability of dilute Mg-based alloys: A first-principles study of shear deformation. *Acta Mater.* **2014**, *67*, 168–180. [CrossRef]

23. Wang, J.; Sehitoglu, H.; Maier, H.J. Dislocation slip stress prediction in shape memory alloys. *Int. J. Plasticity* **2014**, *54*, 247–266. [CrossRef]
24. Cai, T.; Zhang, Z.J.; Zhang, P.; Yang, J.B.; Zhang, Z.F. Competition between slip and twinning in face-centered cubic metals. *J. Appl. Phys.* **2014**, *116*, 163512. [CrossRef]
25. Fu, C.L.; Ye, Y.Y.; Yoo, M.H. Theoretical investigation of the elastic constants and shear fault energies of Ni_3Si. *Philos. Mag. Lett.* **1993**, *67*, 179–185. [CrossRef]
26. Mryasov, O.N.; Gornostyrev, Y.N.; van Schilfgaarde, M.; Freeman, A.J. Superdislocation core structure in L1 NiAl, NiGe and FeGe: Peierls-Nabarro analysis starting from ab-initio GSF energetics calculations. *Acta Mater.* **2002**, *50*, 4545–4554. [CrossRef]
27. Brugger, K. Thermodynamic definition of higher order elastic coefficients. *Phys. Rev.* **1964**, *133*, 1611–1612. [CrossRef]
28. Vinet, P.; Rose, J.H.; Ferrante, J.; Smith, J.R. Universal features of the equation of state of solids. *J. Phys. Condens. Matter* **1989**, *1*, 1941–1963. [CrossRef]
29. Wang, Y.; Wang, J.J.; Zhang, H.; Manga, V.R.; Shang, S.L.; Chen, L.Q.; Liu, Z.K. A first-principles approach to finite temperature elastic constants. *J. Phys. Condens. Matter* **2010**, *22*, 225404. [CrossRef] [PubMed]
30. Shang, S.L.; Zhang, H.; Wang, Y.; Liu, Z.K. Temperature-dependent elastic stiffness constants of α- and θ-Al_2O_3 from first-principles calculations. *J. Phys. Condens. Matter* **2010**, *22*, 375403. [CrossRef] [PubMed]
31. Liu, Z.K.; Zhang, H.; Ganeshan, S.; Wang, Y.; Mathaudhu, S.N. Computational modeling of effects of alloying elements on elastic coefficients. *Scr. Mater.* **2010**, *63*, 686–691. [CrossRef]
32. Kresse, G.; Hafner, J. Ab initio molecular dynamics for open-shell transition metals. *Phys. Rev. B* **1993**, *48*, 3115. [CrossRef]
33. Kresse, G.; Furthmller, J. Efficiency of ab-initio total energy calculations for metals and semiconductors using a plane-wave basis set. *Comput. Mater. Sci.* **1996**, *6*, 15–50. [CrossRef]
34. Kresse, G.; Furthmller, J. Efficient iterative schemes for ab initio total-energy calculations using a plane-wave basis set. *Phys. Rev. B* **1996**, *54*, 11169–11186. [CrossRef]
35. Perdew, J.P.; Burke, K.; Ernzerhof, M. Generalized gradient approximation made simple. *Phys. Rev. Lett.* **1996**, *77*, 3865–3868. [CrossRef] [PubMed]
36. Blöchl, P.E. Projector augmented-wave method. *Phys. Rev. B* **1994**, *50*, 17953–17979. [CrossRef]
37. Kresse, G.; Joubert, D. From ultrasoft pseudopotentials to the projector augmented-wave method. *Phys. Rev. B* **1999**, *59*, 1758–1775. [CrossRef]
38. Monkhorst, H.J.; Pack, J.D. Special points for Brillouin-zone integrations. *Phys. Rev. B* **1976**, *13*, 5188–5192. [CrossRef]
39. Wang, R.; Wang, S.F.; Wu, X.Z.; Liu, A.P. First-principles phonon calculations of thermodynamic properties for ductile rare-earth intermetallic compounds. *Intermetallics* **2011**, *19*, 1599–1604. [CrossRef]
40. Liu, L.L.; Wang, R.; Wu, X.Z.; Gan, L.Y.; Wei, Q.Y. Temperature effects on the generalized planar fault energies and twinnbilities of Al, Ni and Cu: First principles calculations. *Comput. Matter. Sci.* **2014**, *88*, 124–130. [CrossRef]
41. Gülsern, O.; Cohen, R.E. High pressure thermoelasticity of body-centered cubic tantalum. *Phys. Rev. B* **2002**, *65*, 064103. [CrossRef]
42. Nye, J.F. *Physical Properties of Crystals*; Clarendon Press: Oxford, UK, 1964.
43. Paidar, V.; Pope, D.P.; Vitek, V. A theory of the anomalous yield behavior in L12 ordered alloys. *Acta Metall.* **1984**, *32*, 435–438. [CrossRef]
44. Rice, J.R. Dislocation nucleation from a crack tip: An analysis based on the Peierls concept. *J. Mech. Phys. Solids* **1992**, *40*, 239–271. [CrossRef]
45. Wang, T.C.; Wang, K.R.; Zhang, Y.W. A unified model for dislocation nucleation, dislocation emission and dislocation free zone. *Int. J. Fract.* **1996**, *78*, 227–239. [CrossRef]
46. Yoo, M.H.; Fu, C.L.; Horton, J.A. Crack-tip dislocations and fracture behavior in Ni_3Al and Ni_3Si. *Mater. Sci. Eng. A* **1994**, *176*, 431–437. [CrossRef]